IOP Publishing Journal of Physics D: Applied Physics

J. Phys. D: Appl. Phys. **53** (2020) 455103 (9pp) https://doi.org/10.1088/1361-6463/aba4d6

Matched characterization of super-multiperiod superlattices

Leonid Goray[1,2,3], Evgeniy Pirogov[1,4], Maxim Sobolev[1], Igor Ilkiv[1], Alexander Dashkov[1], Ekaterina Nikitina[1], Evgenii Ubyivovk[2], Leonid Gerchikov[1,5], Andrei Ipatov[1,5], Yuliy Vainer[6], Mikhail Svechnikov[6], Pavel Yunin[6], Nikolay Chkhalo[6] and Alexei Bouravlev[1,3]

[1] Alferov University, 8/3 Khlopin Str., Let. 'A', Saint Petersburg 194021, Russia
[2] ITMO University, 49 Kronverkskiy Pr., Saint Petersburg 197101, Russia
[3] Institute for Analytical Instrumentation, 26 Rizhsky Pr., Saint Petersburg 190103, Russia
[4] Connector Optics LLC, 16 Domostroitelnaya Str., Let. 'B', Saint Petersburg 194292, Russia
[5] Peter the Great St Petersburg Polytechnic University, 29 Polytechnicheskaya Str., Saint Petersburg 195251, Russia
[6] Institute for Physics of Microstructures, 7 Academicheskaya Str., Afonino, Nizhny Novgorod region 603087, Russia

E-mail: lig@pcgrate.com

Received 3 May 2020, revised 4 July 2020
Accepted for publication 10 July 2020
Published 11 August 2020

Abstract

Heterostructures with multiple strongly coupled quantum wells, such as super-multiperiod (SMP) superlattices (SLs), are promising semiconductor devices, which may contain hundreds or even thousands of layers with 100 or more periods synthesized by molecular beam epitaxy (MBE) to high structural perfection. The proposed characterization method employs matched application of high-resolution x-ray diffractometry (XRD), reflectometry (XRR), and, for the first time, the deep XRR (DXRR) allows the study of SMP structures, as well as high-accuracy determination of the thicknesses of layers, roughness/diffuseness of boundaries using the rigorous scattering theory, and composition of solid solutions. Combining these methods with scanning transmission electron microscopy (STEM) enables characterization of SMP SLs and independent determination of these same parameters. The differences between the expected and obtained layer thicknesses by XRD and XRR were 1%–3% for AlGaAs/GaAs structures. The samples were characterized by sharp interfaces with the root-mean-square width of the transition layers of the order of a few Å, which is consistent with the XRR/DXRR and STEM analysis. Based on the data obtained for the thicknesses of layers, the composition of $Al_{0.3}Ga_{0.7}As$ has been accurately determined by the x-ray methods. These results may be considered as the first step in the analysis of MBE-grown SMP structures with a number of periods up to 1000.

Supplementary material for this article is available online

Keywords: superlattice, molecular beam epitaxy, x-ray diffractometry, x-ray reflectometry, rigorous electromagnetic theory, transmission electron microscopy

(Some figures may appear in colour only in the online journal)

1. Introduction

Promising semiconductor devices such as quantum-cascade lasers, solar cells and similar heterostructures with multiple strongly coupled quantum wells (QWs) have attracted considerable attention [1–6]. They may operate in the terahertz range and contain hundreds or even thousands of layers, with thicknesses that may vary by orders of magnitude [7–9]. In this

study, the synthesis of 'super-multiperiod' (SMP) superlattices (SLs) with 100 and more periods and/or large-thickness structures with high perfection of the layer morphology and composition is considered in relation to the creation of new near-room-temperature laser sources of infrared and terahertz radiation, including the formation of corresponding minibands (Wannier-Stark energy levels [10]) or sequential tunneling of carriers through many periods [11–14].

An increase in the number of periods leads to the increase of the device output power and decrease of the threshold current of generation. Therefore, to overcome the absorption in a resonator and losses in contact areas, large numbers of SL periods (up to 1000) have to be created; thus, structures with a thickness of 5–10 μm or more are needed [15]. The creation and characterization of SMP structures with a constant period and required doped levels throughout the thickness is a nontrivial task. Difficulties arise because of the electron scattering at interfaces, emergence of various kinds of defects, deep impurity levels, and inconstancy of layer compositions [16]. Therefore, samples should be grown with the thickness accuracy at the atomic level, roughness/diffuseness of interfaces at the subatomic level (root mean square (RMS) σ), and layer composition accuracy of less than a fraction of a percent [17]. In our studies, we deal with weakly stressed structures, such as AlGaAs/GaAs and also InAs/GaAs QWs [18]. Because of the relatively low growth rate of SMP structures using molecular beam epitaxy (MBE), sample growth process takes from several hours to a few days [16]. Therefore, the depletion of sources of semiconductor materials of group 3 during direct synthesis of SMP structures should be considered using *in situ* adjustments for such nonlinear processes, which is possible by the accurate analyses of test samples and calibration of material fluxes *ex situ*.

Among the best integral non-destructive tools for the evaluation of such SLs are the high-resolution x-ray diffractometry (XRD) and (XRR) based on the detailed analysis of specular and diffuse component distributions of the x-ray scattering intensity in reciprocal and direct spaces and exact solution of the inverse problems [19–22]. The XRD and XRR methods are complementary, allowing to avoid the dependence between model parameters, the number of which may reach several hundreds. However, the great opportunities inherent in XRD and XRR may not be fully exploited for a complete characterization of SMP structures because of the difficulties in unambiguously interpreting the data obtained with a large number of free parameters embedded in complex models and using approximations. To overcome these difficulties, we use, for the first time for such structures, the method of deep x-ray reflectometry (DXRR) based on the rigorous scattering model [23]. To clarify the morphology and composition of layers and interface sharpness over the depth of SLs, the transmission electron microscopy (TEM) method is widely used as independent [24]. Another method for determining the structural parameters and composition of samples with multiple QWs is the photoluminescence (PL) spectroscopy [25] which is discussed here in the supplementary material (available online at stacks.iop.org/JPysD/53/455103/mmedia). The methodology of using all the basic methods together for characterizing SMP structures are analyzed in this work.

2. Independent methods

2.1. MBE

In this work, we primarily studied Design II samples grown on 'epi-ready' GaAs (100) substrates using MBE with the semi-industrial Riber 49 and R & D Riber Compact 21 EB 200 systems. The other Design SLs, which were grown and investigated by the same methodology, are mentioned here briefly. Design II structure included an SL of 100 periods consisting of $Al_{0.3}Ga_{0.7}As$ (15 nm)/GaAs (3 nm) layers with the cupping layer of GaAs of thickness of 10 nm. The thickness of Design II structure was approximately 1.8 μm. The quality of layers was controlled *in situ* by the diffraction of high-energy reflected electrons. In addition, the ability to create an abrupt interruption and then resume allowing molecular beams to enter the substrate allows for the production of sharp heterointerfaces, which is crucially important for creating SMP structures with QWs. Moreover, such equipment can maintain highly stable source temperatures, which ensures the consistency of compositions. Using these MBE systems, it is possible to synthesize high-quality layers with a thickness of one monolayer, as well as very thick layers while controlling thickness and composition [26, 27]. Samples of Design II were studied in detail by XRD and XRR/DXRR, and, additionally, by scanning TEM (STEM).

Design I structure of approximately 1.5 μm thickness consisted of 10 periods of InAs/GaAs multilayers and a cupping layer of GaAs with a thickness of 10.3 nm [18].

Design III structure included SLs of 100 periods consisting of $Al_{0.3}Ga_{0.7}As$ (2 nm)/GaAs (10 nm) layers without impurities and doping by *n*-type impurities of different concentrations. The thickness of Design III structure was approximately 1.2 μm. Design III will be discussed elsewhere.

2.2. XRD

For measuring the structures with different numbers of periods which consist of several layers with similar periods, a target growth model was used. The software embedded in the universal XRDs was used to solve the inverse problem of XRD, namely, 'Epitaxy' and 'Smoothfit' were used for PANanalytical X'Pert Pro [28], and DIFFRAC.Leptos was used for Bruker AXS [29]. These proprietary software products are designed to solve the Takagi-Taupin equations [30] and use genetic algorithms to search for local minima in the model parameter space. Further, using the local minima found with the gradient descent method (or the Levenberg–Marquardt method), it is possible to find a global minimum. In addition, these software products incorporate various models to consider the roughness and diffuseness of interfaces (transition

layers). Furthermore, these software products provide opportunities to improve the model and assess its reliability as well as the accuracy of curve-fitting.

Design II structure was investigated using the XRD method on a Bruker D8 Discover XRD (Cu $K\alpha_1$ radiation) configured in the scheme with the Goebel parabolic mirror and Ge (220) double-reflection monochromator on the primary beam. To determine the SL period, a diffraction reflection curve was taken near the (002) GaAs and (004) GaAs reflections by θ–2θ scanning with a slit with $\omega = 1$ mm in front of the detector in the ranges of angles from 23° to 70° over 2θ with the step of 0.01° and the accumulation time of 2 s.

The composition of the AlGaAs solid solution was determined from the position of the zero peak of the SL near the (004) GaAs reflection; the preliminary determined ratio of the thicknesses of the individual layers in the period was considered. To accomplish this, a rocking curve was taken in a small range of angles from 32.9–33.1° along θ with a step of 0.001° and a wide slit on the detector $\omega = 4.5$ mm.

2.3. XRR

To reconstruct the morphology of SMP structures with the help of XRR, one may use 'model', 'model-less' or 'hybrid' approaches [22, 31, 32] and also consider additional independent methods (XRD, TEM, PL, others). The use of *a priori* information about the flows and growth times of layers with regard to their depletion [16] is also necessary for an initial approximation in the procedure of fitting theoretical data to experimental data and significant reduction of the number of reconstructed parameters. For solving the inverse problem of restoring the parameters of layers by XRR the homemade code 'Multifitting' was used [33].

Multifitting is a computer program designed specifically for modeling the optical properties (reflection, transmission, absorption) of multilayer films consisting of an arbitrary number of layers in a wide range of wavelengths. Multifitting allows a user to calculate the reflectometric curves for a given structure (direct problem) and to find the parameters of the films from the experimentally obtained curves (inverse problem), either manually or automatically. Key features of Multifitting are the ability to work simultaneously with an arbitrary number of experimental curves and an ergonomic graphical user interface that is designed for intensive daily use in the diagnosis of thin films. Multifitting is positioned as the successor to the IMD program [31], which has become the standard tool in research and technology groups synthesizing and studying thin-film coatings.

Reflectometric measurements were performed on a PANalytical X'Pert Pro diffractometer in the θ–2θ mode at grazing incidence angles in the range 0–3.4°. In the range of small angles (0–1.8°), a 0.2 mm slit was used, the scanning step was equal to 0.001°, and the recording time for one reflex was 4 s. For large angles, the slit was 0.8 mm wide, the step was 0.001°, and the recording time was 7 s.

2.4. STEM

The TEM method is another independent quantitative approach to check the validity of the mentioned above methods. We studied the same samples using the TEM method to obtain additional quantitative information on the thickness and composition of SL layers.

The samples for TEM studies were prepared by the focused ion beam method using the Zeiss Auriga Crossbeam system [34]. The obtained lamellas were studied on the TEM Zeiss Libra microscope with an accelerating voltage of 200 kV in the STEM mode by employing a procedure similar to that described in [35]. Microscopic measurements and assessments were carried out in three SL areas of SMP Design II structure: in the lower, near the substrate; in the middle, near the SL center; and in the upper, near the cupping layer.

3. Deep XRR: theoretical model

To study the SMP structures, along with usual XRD and XRR, we used first the DXRR method [36], which is a principal improvement of XRR because of the possibility of expanding the ranges of input and analyzed parameters by an order of magnitude without loss of accuracy, which is crucial for the analysis of thick SMP structures. Even specular reflectances of x-ray radiation at boundaries with random roughnesses may differ considerably (by orders of magnitude) from the values derived with the use of various approximate models [37]. The general DXRR method has already been successfully applied to the analyses of multilayer crystalline and amorphous samples of large thicknesses [38–40].

This approach is based on the rigorous theory of diffraction of electromagnetic radiation, namely, the modified boundary integral equation method together with the method of Monte Carlo to take into account a boundary randomization [23, 38]. It can describe different situations from total external reflection to full absorption of short-wave radiation; in addition, it enables accurate determination of the intensity of scattered light and absorption.

The DXRR method is suitable to solve rigorously any direct problem of reflectometry and also to check a validity of a plethora of approximations, which are traditionally used in XRR. As a result, it allows verification of methods to analyze SMP structures with the thickness from a few to 10 and even more microns, when measured at very bright x-ray free electron lasers or synchrotron radiation (SR) sources of the fourth generation. It was also recognized that the method of DXRR operates equally well with any shape of asperities and allow arbitrary statistics of distribution: periodic, quasi-periodic, random, as well their combinations including realistic (measured or simulated) [41, 42].

In the strict sense, the Debye-Waller (DW) and Nevot-Croce (NC) factors of the reduction in specular reflectance are valid in the case of small rough boundary heights h (or σ) having a Gaussian distribution and very large (DW) or very small (NC) correlation lengths ζ. The second order distorted-wave

Born approximation may be used while considering arbitrary magnitudes of ζ. However, it is generally valid for very small values of $2\pi\sigma \sin\theta/\lambda$ and when the Gaussian-like correlation function is used [43, 44]. Additionally, derivations of the NC factor assume ζ satisfying $\lambda \gg 2\pi\zeta \sin^2\theta$. For the case studied that means $\sigma \ll 5$ nm and $\zeta \ll 900$ nm. The real situation is more complex and the result depends also significantly on real and imaginary parts of the refractive index.

The height perturbation theory is more general because any height distribution and any correlation function can be used via the power spectral density function; however, it also has strong restrictions, mainly, in the allowed maximal height values [45–49]. The big difference (up to an order of magnitude) between the rigorous approach and the DW & NC approximations was clearly demonstrated in specular reflectances of Au mirrors with different roughness parameters at wavelengths where grazing incidences occur at close to or larger than the critical angles [37]. Such differences may give rise to wrong estimates of σ and ζ (and also layer thicknesses) if they are obtained in XRR by comparing experimental data with calculations.

Thus, rigorous-based DXRR computations are required to find limitations and errors of the usual XRR model applied to a particular case. By the same rigorous approach, EUV specular and diffuse reflection coefficients were calculated for Al/Zr multilayers accounting for real (non-Gaussian) rough boundary statistics [40]. The complex multilayer model [50], which considers the exact effects of growth kinetics of boundaries having random roughnesses with varying σ and ζ, has demonstrated very good correlation of specular reflectance values with the data obtained on the SR source for a number of incidence angles and wavelengths.

The rough surface statistics is required to rigorously compute the scattering intensity using the direct electromagnetic solver PCGrate™-SX v. 6.7 [51]. For this purpose, we employ Monte Carlo simulations to average the statistics owing to individual surfaces over an ensemble of realizations. Here, we can use a model of vertically uncorrelated roughnesses due to a variable random noise of material sources and small σ (approximately a few Å) of the substrates [38, 52]. In this case, the specular reflection of an SL is proportional to the intensity of the specular field at the interfaces. Moreover, the simple evaluation shows that the angular distribution of the scattered intensity is characteristic of scattering from a single interface [53]. Therefore, we may study in detail only one rough GaAs surface to compare calculation results obtained using DXRR (rigorously) while applying NC and DW attenuation factors, which are mostly used to solve inverse XRR problems.

4. Results and discussion

The positions of the maxima on the XRD curves (figure 1) correspond to the diffraction peaks from the GaAs substrate, to the average composition of the SL; and the distance between the peaks (satellites) corresponds to the period D of the SL [54]. The satellite structure is observed in a wide angular range on a double scale of Bragg angles, which indicates high quality, planarity, and continuity of the layers that form the periodic structure. The structure was calculated with the full thickness of grown layers and $D = 17.5$ nm. In the diffraction pattern, there is a large number of satellite peaks due to a good contrast, resulting from the difference in atomic factors of Ga and Al. It should be noted that the satellites have a clearly defined shape with one maximum. In the case of non-optimized parameters of the epitaxial process, both the splitting of satellite peaks and presence the of several maxima are possible. This is associated with fluctuations in the composition and thickness of epitaxial layers in the structure [16, 26]. Further, the SL period and thicknesses of individual layers in the period were determined from the envelope shape of the satellites and their positions determined by fitting a theoretical curve. The period was determined as $D = 17.5 \pm 0.2$ nm, and the thicknesses of the layers were found as d(GaAs) = 3.0 nm and d(AlGaAs) = 14.5 nm.

Table 1. Restored thickness parameters.

Design II				
SL Layer	XRD, nm	XRR, nm	Matched, nm	σ, nm, XRR
GaAs	3.0	3.0	3.0	0.35
$Al_{0.3}Ga_{0.7}As$	14.5	14.55	14.55	0.35
D	17.5 ± 0.2	17.55 ± 0.05	17.55 ± 0.05	

The diffractometry analysis results showed that D of the grown structure was 2.8% less than the expected value, and d(AlGaAs) was less by 3.3% (see figure 1(a)). From the attenuation of satellites at large distances, we estimated the fluctuation of D as 0.2 nm. Figure 1(c) presents the diffraction spectrum taken near the GaAs (004) reflection, for which the fitting also confirms $D \approx 17.55$ nm. Quantitative assessment of the match between measured and simulated XRD diffraction curves was evaluated using the DIFFRAC.Leptos built-in normalized logarithmic discrepancy functional χ^2 [29]: $\chi_{LN}{}^2 = 1/N \cdot \Sigma\ ((\log(I_{exp}) - \log(I_{sim}))/\log(I_{exp}))^2$, where I_{exp} is measured intensity and I_{sim} is simulated one. The sum is taken over the all spectrum data points N. Minimization of normalized logarithmic χ^2 is a conventional approach to fitting of XRD spectra [55, 56].

To verify the XRD model and to determine the absolute errors for this structure, the XRR method was used. In the resulting model of XRR, the following values were obtained for the best agreement with the experimental data (figure 2): $D = 17.55$ nm, $d(Al_{0.3}Ga_{0.7}As) = 14.55$ nm, d(GaAs) = 3.0 nm. The difference between period thickness determined from XRD and XRR lies inside the XRD tolerance (0.2 nm). D(XRR) $= 17.55 \pm 0.05$ nm is the most strict value derived from these two methods. Applying the XRR method, after the XRD method, allows to restrict the average period determination error to 0.05 nm only. Moreover, now we can assume the absolute error due to the use of the two independent methods. The combined thickness parameters and errors obtained by the two methods under examining Design II structure are listed in table 1.

The thickness of the upper GaAs cap layer was d(GaAs) = 9.92 nm, and it turned out to be not oxidized.

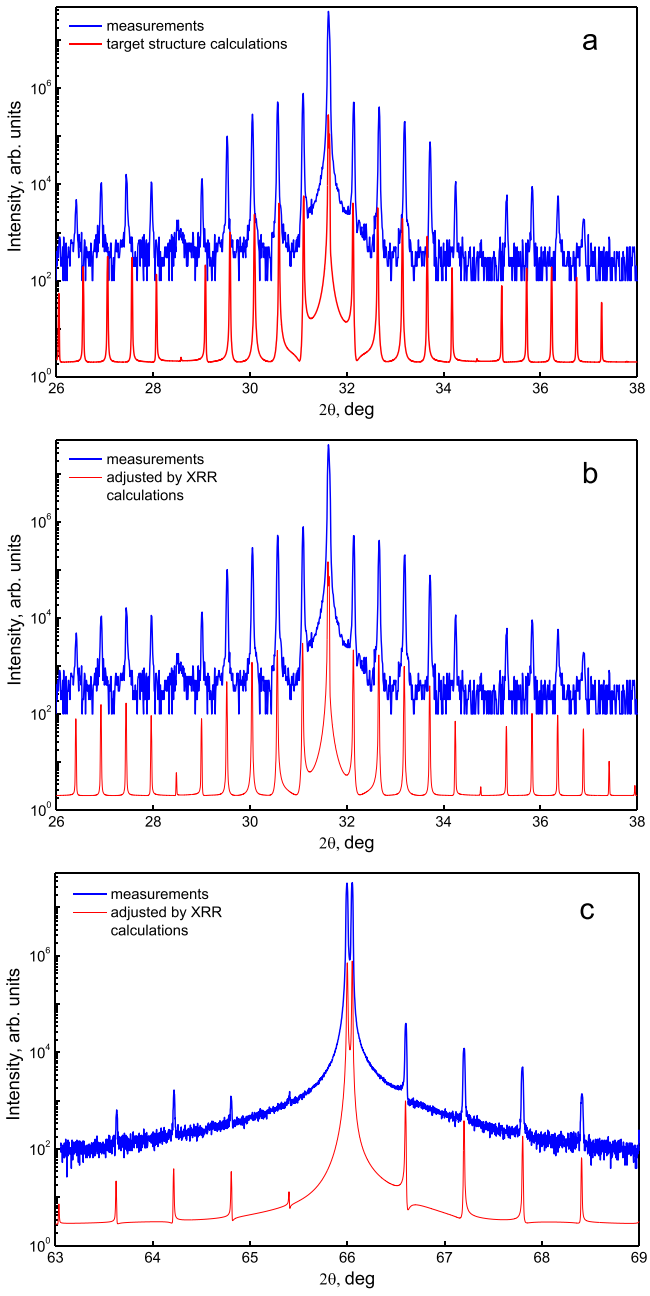

Figure 1. XRD curves of Design II structure with 100 periods obtained in the θ-2θ scan mode at the wavelength $\lambda = 0.15406$ nm with (a, b) near the (002) GaAs reflection and (c) near the (004) GaAs reflection (the curves are shifted for clarity).

The width of the interfaces of layers was $\sigma = 0.35$ nm in the symmetrical interface model. The resulting XRR model provided a perfect match between the experimental and theoretical peaks for 10 diffraction orders, which indicates high quality of the structure and good fit. Then, applying successively XRD after XRR we finally obtain perfectly matched XRD curves, which are also matched in the best way to XRR data (see figures 1(b) and (c)). Such a methodology can be (and should be) applied to any design of SMP structures [18].

Exact calculations of the scattered light intensity were performed using DXRR for the interface roughness with

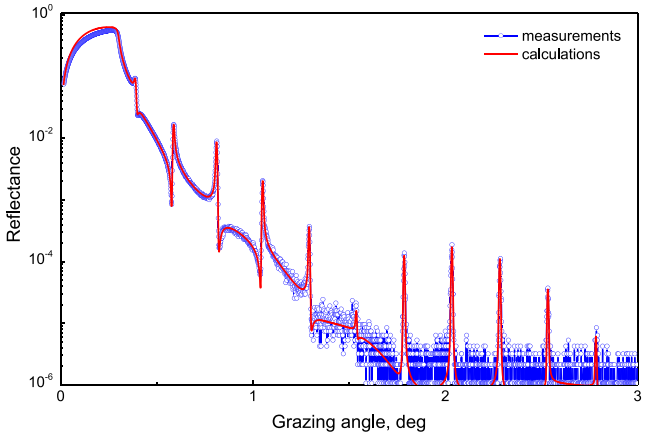

Figure 2. Specular reflectance of Design II structure with 100 periods obtained for the wavelength $\lambda = 0.15406$ nm vs. grazing angle.

different σ: 0.35 nm, 0.7 nm and 1.5 nm. Any correlation length evaluated had values close to those given by either the DW model ($\zeta = \infty$), or the NC model (or the more general Sinha's approximation [57]) ($\zeta = 0$), or more realistic models ($\zeta = 0.15$ μm, 1.5 μm, 15 μm) in the entire grazing incidence angle range. The calculated specular TE reflectance (TM reflectance data are close in magnitude) of GaAs surfaces as a function of the angle of incidence for different values of σ and ζ is shown in figure 3. A comparison of the reflectance obtained for Cu K_α radiation ($\lambda = 0.1541$ nm) for the approximate (NC and DW) and perfect ($\sigma = 0$) models and for the rigorous model ($\sigma = 1.5$ nm) for different ζ values is shown in linear (near the critical angle in figure 3(a)) and logarithmic (in the wide angular range in figure 3(b)) scales. One can clearly see the difference between results obtained using the rigorous approach and the approximated approaches.

We will first discuss the results for the cases when the incidence angle is close to the critical angle (see figure 3(a)). For $\zeta = 0.15$ μm, the results obtained for the rigorous and NC model differ only by a few % near and below the critical angle, and by several % in the range slightly higher the critical angle. For $\zeta = 1.5$ μm, the difference is several % in the high reflectance range, and approximately a few tens of % in the low reflectance range. For $\zeta = 15$ μm, the difference is approximately a few tens of % in the high reflectance range, and approximately several tens of % or a few times in the low reflectance range; similar differences can be observed for $\zeta = 15$ μm and the DW model. For $\sigma = 0.7$ nm, the NC model (not shown) is close (with the maximal difference of several %) to the perfect reflectance, and also to the rigorous model with the highest value of ζ (=15 μm). For $\sigma = 0.35$ nm, all the models are very close (with the maximal difference of only a few %) in the considered incidence angle range.

When the incidence angle is much higher than the critical angle, the results obtained by the different models vary to a much greater degree (see figure 3(b)). For $\sigma = 1.5$ nm, while the rigorous results obtained for various ζ are close, they are distant from the predictions made by both DW and

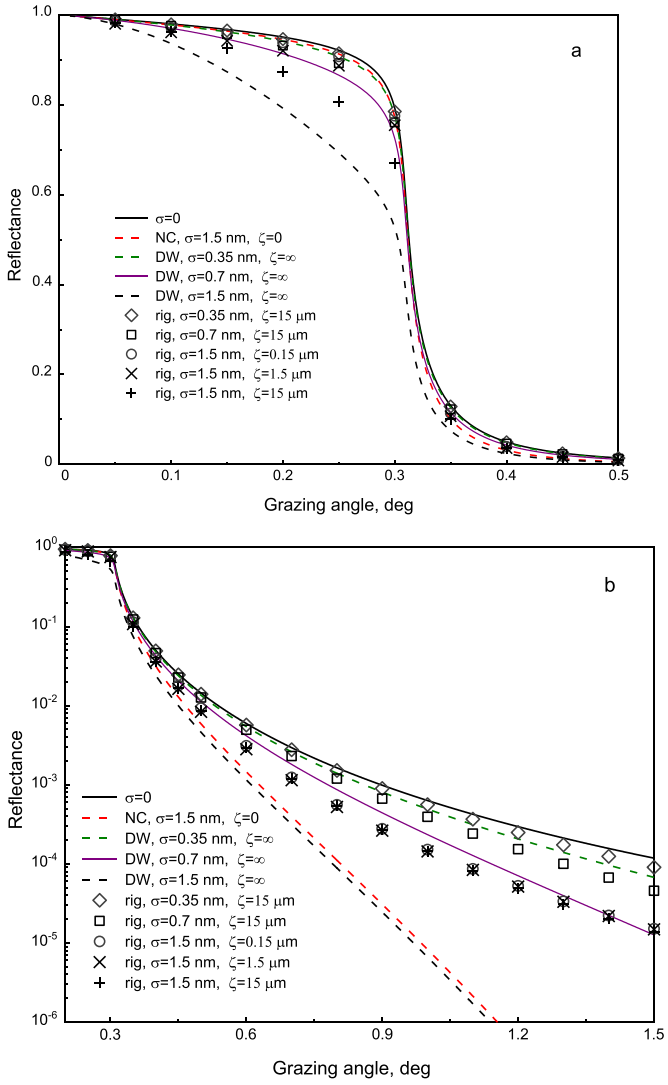

Figure 3. Specular reflectance of GaAs as a function of grazing angle. Specular reflectance calculated by approximations (NC or DW curves) and rigorously (symbols) with 99 statistical surface realizations for the wavelength $\lambda = 0.1541$ nm and different rms roughness σ and correlation length ζ: (a)—in linear scale near the critical angle; (b)—in logarithmic scale in the wide-angle range.

NC approximations. For example, when $\theta = 0.9°$, the results differ by nearly an order of magnitude; at higher values of θ, the differences are even larger with a few orders of magnitude between the values obtained. For $\sigma = 0.7$ nm and $\zeta = 15$ μm, the rigorous results are rather close to the DW predictions. However, the difference varies from several tens of % up to a few times in the range under consideration. For $\sigma = 0.35$ nm and $\zeta = 15$ μm, it is seen that the rigorous results are close to the DW predictions; in this case, the difference varied from several % to several tens of % in the range under study.

The results presented in figure 3 exhibit good convergence and high accuracy required for simulating specular reflectance of SLs with polygonal and randomly rough boundaries that have 1000 nodes; a wide angular range is also employed for the simulation. In PCGrate, we used 1000–1200 discretization points per boundary, 99–195 random boundary sets, and the Separating solver after excluding the convergence acceleration technique. An error of approximately 1.E–6 that accounts for exact absorption calculus was evaluated from energy balance considerations [23]. The difference between reflectances obtained using 99 and 195 random boundary sets is approximately 0.1%. The difference between reflectances obtained using 49 and 195 random boundary sets is approximately (or less than) 10%. The average time taken by each discretization point (99 random sets) on a portable workstation MSI® WT73VR 7RM with an Intel® Xeon® E3-1505M V6 3–4 GHz processor and 64 GB of RAM is approximately 4 h when operating on Windows® 10 Pro using eight-fold parallelization. The GaAs refractive indices were derived from the CXRO website [58].

As predicted by the general theory, the rigorous results for small values of σ and ζ are close to the NC model near and below the critical angle. In the range higher than the critical angle, as would be expected, the rigorous results may be close to those of the DW or NC model only for small values of σ (less than or about approximately 0.35 nm for the considered case) and various values of ζ. For higher values of σ, pronounced differences between the rigorous model and any widely used approximations may result in an overestimation of σ if it is deduced from a comparison of experimental data with calculations.

Thus, for Design II structure the usual XRR approximation with $\sigma \approx 0.35$ nm provide accurate results for all correlation lengths and incidence angles studied. The inaccuracy of the obtained specular reflectance results is approximately 1%. The respective inaccuracy of the restored layer thicknesses is also about 1%. For Design II structure, the XRR approximation give accurate results for all boundaries in the wide incidence angle and correlation length ranges.

Similar to Design I sample [18], Design II sample was elastic-stressed and convex with the SMP layer outward. To calibrate the reflected radiation intensity, I, with the intensity of the incident radiation, I_0, measurements were taken at zero degrees to collect all the radiation from the source outside the critical angle. The measurements were carried out with different slit widths $\omega = 0.03$ mm, $\omega = 0.1$ mm, $\omega = 0.2$ mm, and $\omega = 0.8$ mm; the angle scan step was 0.001° and the exposure time was 3 s. At small angles (0–1.8°), the slit width was 0.2 mm, the scanning step was 0.001°, and the scan time per point was 4 s. At large angles, the slit width was 0.8 mm, the step was 0.001°, and the scan time was 7 s. Figure 4 presents the x-ray reflectometry curves obtained using wide slits in front of the detector to analyse the radiation reflected in a wide range of angles.

Using glancing angles smaller than the critical angle together with a narrow slit created a configuration that did not allow a for reflection close to 100%. The radius of the measured structure (including the outer convex layer of the SMP structure) was ~50 m, corresponding to a total structural stress of around 8×10^7 Pa, which is not critical for thin layers and does not lead to the generation of dislocations [59].

The next step in the matched procedure was to determine the proportion x of Al in the $Al_xGa_{1-x}As$ layers.

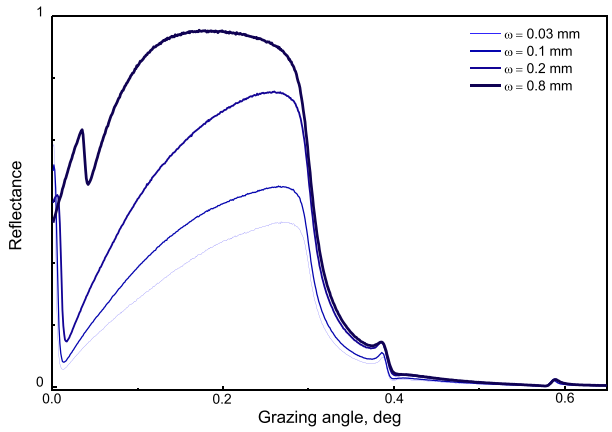

Figure 4. Intensity of the specular reflection $R = I/I_0$ of Design II sample measured near the total external reflection with the slit width ω for the incident radiation with $\lambda = 0.15406$ nm vs. grazing angle.

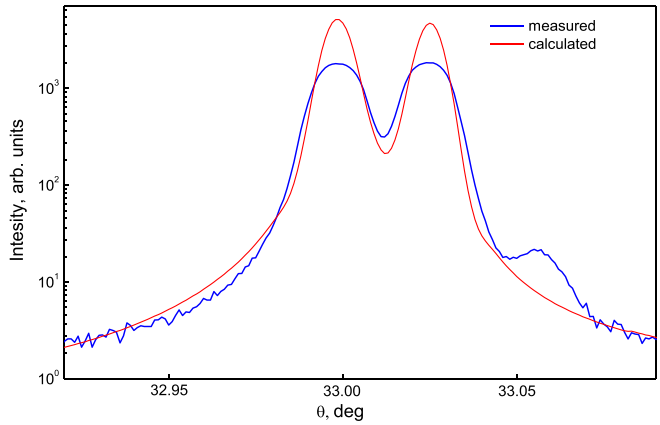

Figure 5. Rocking curve of Designe II sample obtained near the (004) GaAs reflex in a small range of angles on θ.

The rocking curve obtained near the (004) GaAs reflex in a small range of angles on θ is demonstrated in figure 5. Two intense peaks are observed on the spectrum. The right peak corresponds to the substrate material GaAs (004), and the left peak corresponds to the average composition of the SL. The low-intensity peak on the right is an artifact of a double monochromator; thus, it was not considered. The average composition was determined by the formula:

$$< \mathrm{x} > = \frac{x(\mathrm{AlGaAs}) \cdot d(\mathrm{AlGaAs})}{D}. \qquad (1)$$

Since the period D and layer thickness d were determined from the spectrum of XRD near the (002) reflection, only the value of x(AlGaAs) varied in the process of fitting the calculated curve. The resulting proportion of Al was $x = 0.3 \pm 0.005$ that is closely matched to the growth model.

Figure 6 shows the high-angle annular dark-field (HAADF) of a sample obtained using STEM, indicating a high degree of perfection of the SL. Figure 7 shows the HAADF image of

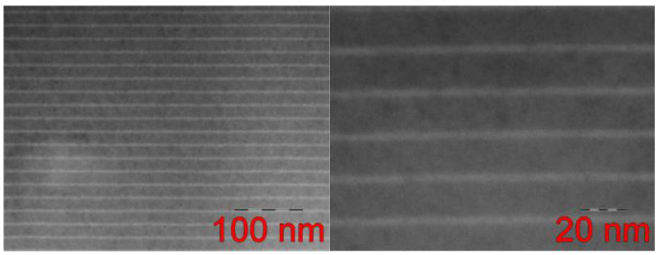

Figure 6. HAADF-STEM images an SL sample obtained with different resolutions.

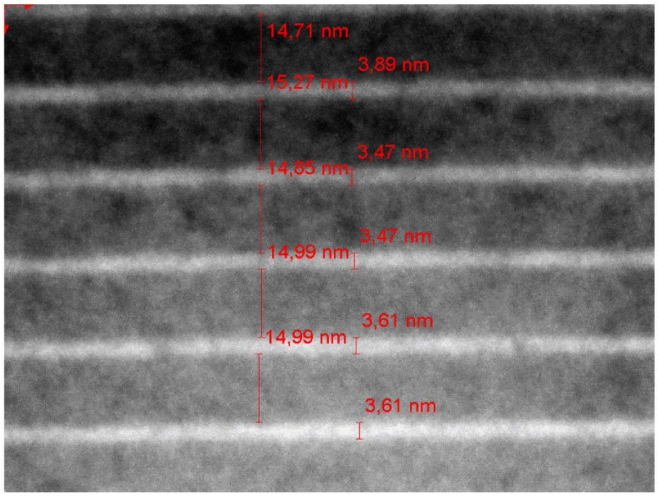

Figure 7. HAADF-STEM image of an SL sample with measured bars.

a similar sample with bars indicating the thicknesses of layers, including transition ranges with the random roughness and intermixing of layers. The thicknesses of the layers in the STEM image were measured approximately, since the thickness of the sample was quite large and, therefore the boundaries of the layers did not have a clear contrast.

According to the measurement data for several samples, σ is about 0.5 nm in the approximation of symmetric interfaces. Considering the calibration error of microscopic measurements (approximately 0.25 nm), the STEM data on the thicknesses of layers quantitatively agree with the results obtained using XRD and XRR. Due to the large measurement error in determining the thickness on the STEM image lad to discrepancy of ∼8% between the XRD/XRR and the STEM measurements. However, choosing the bars, which indicate the thicknesseses of layers, is rather voluntarist.

5. Conclusion

The research methods herein, including XRD, XRR, DXRR, and STEM, are suitable for analyzing SMP structures and allow for sample characterization and determination of parameters such as thicknesses and layer composition with high validity and accuracy. The differences between the expected and obtained data matched XRD and XRR methods layer

thicknesses were 1%–3% for samples of Design II & III. These differences are likely governed by a decreased flow of group 3 material sources during the growth process of thick structures, which must be compensated for during the time-consuming and expensive experiment. As follows from the theoretical estimates [60], for very thinly deposited layers, thickness calculations, with both compensated and accumulated error types, may have errors that differ by an order of magnitude [18]. The closing speed of the shutter and residual amount of material and its uniformity in the chamber also impact the variation in layer thickness and width of transition regions. According to the XRR data, the structures are characterized by sharp interfaces with σ of the order of a few Å, which was confirmed by STEM measurements.

Based on the rigorous reflectometry model, the DXRR method should be used to check the validity of XRR results, which may differ by orders of magnitude. For example, the XRR results for Design I structure provide overestimated values of σ for several interfaces [18]. In contrast, with Design II & III structures, the inaccuracy of the derived results for $\sigma = 0.35$ nm is only about 1% for all the layers studied. However, this value of σ is close to the critical (before an overestimation) one for Design II structure. Fortunately, the usual XRR approximations with $\sigma \approx 0.35$ nm provide accurate results for all correlation lengths and incidence angles.

STEM analyses can provide valuable additional information and can serve as starting points for matched XRD and XRR. The difference between the expected and resulting average values of the thickness and composition of layers obtained by the XRD & XRR and STEM methods was approximately 8% for samples of Design II. The results obtained in this work demonstrate that the STEM method potentially provides independent quantitative information on the thickness and composition of SL layers, which is often necessary when solving complex inverse problems of XRD and XRR. Based on the available independent data, one can find the best solution of the XRD and XRR problems, and, in turn, determine the morphology and composition of layers of SMP structures with high reliability and accuracy.

Notably, SMP structures with 300–400 and even 1000 periods (Design III) have been grown using our MBE technique; they are currently being investigated by the proposed matched method and by using bright x-ray sources. Thus, the present research is considered as the first main step in obtaining and analyzing SMP heterostructures with very large numbers of periods and large thicknesses.

Acknowledgments

This work was partially supported by the Ministry of Education and Science of the Russian Federation (Minobrnauka) (Grant No. FSRM-2020-0008) and the Russian Foundation for Basic Research (RFBR) (Grant No. 19-29-12053) in part of experimental investigations. The work of L Goray, E Pirogov, M Sobolev and A Dashkov was supported by the Russian Science Foundation (RSF) (Grant No. 19-12-00270) in the theoretical part. The STEM data was obtained using the equipment of the Interdisciplinary Resource Centre for Nanotechnology of St. Petersburg State University, Russian Federation.

ORCID iDs

Leonid Goray https://orcid.org/0000-0002-0381-9607
Igor Ilkiv https://orcid.org/0000-0001-8968-3626
Leonid Gerchikov https://orcid.org/0000-0001-5814-032X
Andrei Ipatov https://orcid.org/0000-0003-1457-8236
Alexei Bouravlev https://orcid.org/0000-0002-7432-2091

References

[1] Köhler R, Tredicucci A, Beltram F, Beere H E, Linfield E H, Davies A G, Ritchie D A, Iotti R C and Rossi F 2002 *Nature* **417** 156
[2] Gmachl C, Sivco D L, Colombelli R, Capasso F and Cho A Y 2002 *Nature* **415** 883
[3] Wacker A 2002 *Phys. Rep.* **357** 1
[4] Courel M, Rimada J C and Hernández L 2013 *Prog. Photovolt., Res. Appl.* **21** 276
[5] Courel M, Rimada J C and Hernández L 2012 *J. Appl. Phys.* **112** 054511
[6] Courel M, Rimada J C and Hernández L 2012 *Appl. Phys. Lett.* **100** 073508
[7] Walther C, Fisher M, Scalari G, Terazzi R, Hoyler N and Faist J 2007 *Appl. Phys. Lett.* **91** 131122
[8] Scalari G, Terazzi R, Giovannini M, Hoyler N and Faist J 2007 *Appl. Phys. Lett.* **91** 032103
[9] Kumar S, Hu Q and Reno J L 2009 *App. Phys. Lett.* **94** 131105
[10] Wannier G H 1960 *Phys. Rev.* **117** 432
[11] Altukhov I V *et al* 2016 *J. Exp. Theor. Phys. Lett.* **103** 122
[12] Amanti M I, Scalari G, Terazzi R, Fischer M, Beck M, Faist J, Rudra A, Gallo P and Kapon E 2009 *New J. Phys.* **11** 125022
[13] Andronov A A, Dodin E P, Zinchenko D I, Nozdrin Y N, Ladugin M A, Marmalyuk A A, Padalitsa A A, Belyakov V A, Ladenkov I V and Fefelov A G 2015 *J. Exp. Theor. Phys. Lett.* **102** 207
[14] Unuma T and Maeda S 2019 *Appl. Phys. Express* **12** 041003
[15] Andronov A A, Dodin E P, Zinchenko D I, Nozdrin Y N, Marmalyuk A A and Padalitsa A A 2010 *Quantum Electron.* **40** 400
[16] Asahi H and Horikoshi Y (eds) 2019 *Molecular Beam Epitaxy: Materials and Device Applications* (New York: Wiley)
[17] Fewster P F 1986 *Philips J. Res.* **41** 268
[18] Goray L I, Pirogov E V, Sobolev M S, Ilkiv I V, Dashkov A S, Vainer Y A, Svechnikov M V, Yunin P A, Chkhalo N I and Bouravlev A D 2019 *Semiconductors* **53** 1914
[19] Pietsch U, Holy V and Baumbach T 2004 *High-Resolution X-Ray Scattering: From Thin Films to Lateral Nanostructures* (Berlin: Springer)
[20] Punegov V I, Pavlov K M, Karpov A V and Faleev N N 2017 *J. Appl. Cryst.* **50** 1256
[21] Borcha M, Fodchuk I, Solodkyia M and Baidakova M 2017 *J. Appl. Cryst.* **50** 722
[22] Kozhevnikov I V, Peverini L and Ziegler E 2012 *Phys. Rev.* B **85** 125439
[23] Goray L I and Schmidt G 2014 Boundary integral equation methods for conical diffraction and short waves *Gratings:*

Theory and Numerical Applications chapter 12 2nd edn, ed E Popov (Marseille: Presses Universitaires de Provence)
[24] Williams D B and Carter C B 2009 *Transmission Electron Microscopy: A Textbook for Materials Science* 2nd edn (Berlin: Springer)
[25] Wojcik-Jedlinska A, Wasiak M, Kosiel K and Bugajski M 2009 *Opt. Appl.* **2009** 967
[26] Pozina G *et al* 2015 *Sci. Rep.* **5** 14911
[27] Pozina G *et al* 2017 *Phys. Status Solidi* B **254** 1600402
[28] Malvern Panalytical™ webpage 2020 Epitaxy & Smoothfit software (www.malvernpanalytical.com/en/products/technology/x-ray-diffraction/high-resolution-x-ray-diffraction/index.html)
[29] Bruker™ webpage 2020 LEPTOS software (www.bruker.com/products/x-ray-diffraction-and-elemental-analysis/x-ray-diffraction/xrd-software/leptos.html)
[30] Takagi S 1962 *Acta Cryst.* **15** 1311
[31] Windt D L 1998 *Comput. Phys.* **12** 360
[32] Svechnikov M, Pariev D, Nechay A, Salashchenko N, Chkhalo N, Vainer Y and Gaman D 2017 *J. Appl. Cryst.* **50** 1428
[33] Svechnikov M 2019 *J. Appl. Cryst.* **53** 244
[34] Ubyivovk E V, Boltynjuk E V, Gunderov D V, Churakova A A, Kilmametov A R and Valiev R Z 2017 *Mater. Lett.* **209** 327
[35] Medvedev O S, Vyvenko O F, Ubyivovk E V, Shapenkov S V and Seibt M 2019 *AIP Conf. Proc.* **2064** 040003
[36] Goray L I, Asadchikov V E, Roshchin B S, Volkov Y O and Tikhonov A M 2019 *OSA Contin.* **2** 460
[37] Goray L I 2010 *J. Appl. Phys.* **108** 033516
[38] Goray L I, Chkhalo N I and Tsyrlin G E 2009 *Tech. Phys.* **54** 561
[39] Goray L I, Chkhalo N I and Vainer Y A 2010 *Tech. Phys. Lett.* **36** 108
[40] Goray L and Lubov M 2015 *Opt. Express* **23** 10703–13
[41] Goray L and Lubov M 2013 *J. Appl. Cryst.* **46** 926
[42] Goray L I 2009 *Proc. SPIE* **7390** 73900V
[43] de Boer D K G 1995 *Phys. Rev.* B **51** 5297
[44] de Boer D K G 1996 *Phys. Rev.* B **53** 6048
[45] Ogilvy J A 1987 *Rep. Prog. Phys.* **50** 1553
[46] Kozhevnikov I V and Pyatakhin M V 2000 *J. X Ray Sci. Technol.* **8** 253
[47] Yashchuk V V, Samoylova L V and Kozhevnikov I V 2015 *Opt. Eng.* **54** 025108
[48] Spiller E 1988 *Rev. Phys. Appl.* **23** 1687
[49] Spiller E 1994 *Soft X-Ray Optics* (Bellingham: SPIE)
[50] Lubov M and Goray L 2019 *J. Synchrotron Rad.* **26** 1539
[51] IIG Inc (www.pcgrate.com)
[52] Stearns D G 1992 *J. Appl. Phys.* **71** 4286
[53] Stearns D G, Gaines D P, Sweeney D W and Gullikson E M 1998 *J. Appl. Phys.* **84** 1003
[54] Bowen D K and Tanner B K 1998 *High Resolution X-Ray Diffractometry and Topography* (Boca Raton, FL: CRC Press)
[55] Ulyanenkov A and Sobolewski S 2005 *J. Phys. D: Appl. Phys.* **38** A235
[56] Yunin P A, Drozdov Y N, Drozdov M N, Novikov A V, Yurasov D V, Zakharov N D and Korolev S A 2014 *Tech. Phys.* **59** 402
[57] Sinha S K, Sirota E B, Garoff S and Stanley H B 1988 *Phys. Rev.* B **38** 2297
[58] Center of X-Ray Optics (http://henke.lbl.gov/optical_constants/)
[59] Kuznetsov G F 2009 *Semiconductors* **43** 472
[60] Spiller E and Rosenbluth A E 1986 *Opt. Eng.* **25** 954